Dynamic coherence analysis of resting fMRI data to jointly capture state-based phase, frequency, and time-domain information

Maziar Yaesoubi[a,b,1], **Elena A. Allen**[a,c,d], **Robyn L. Miller**[a], and **Vince D. Calhoun**[a,b]

[a]The Mind Research Network, 1101 Yale Blvd NE, Albuquerque, New Mexico 87106

[b]Dept. of ECE, MSC01 1100, 1 University of New Mexico, Albuquerque, New Mexico 87131

[c]K. G. Jebsen Center for Research on Neuropsychiatric Disorders, Bergen, Norway

[d]Institute of Biological and Medical Psychology, University of Bergen, Bergen, Norway

Abstract

Many approaches for estimating functional connectivity among brain regions or networks in fMRI have been considered in the literature. More recently, studies have shown that connectivity which is usually estimated by calculating correlation between time series or by estimating coherence as a function of frequency has a dynamic nature, during both task and resting conditions. Sliding-window methods have been commonly used to study these dynamic properties although other approaches such as instantaneous phase synchronization have also been used for similar purposes.

Some studies have also suggested that spectral analysis can be used to separate the distinct contributions of motion, respiration and neurophysiological activity from the observed correlation. Several recent studies have merged analysis of coherence with study of temporal dynamics of functional connectivity though these have mostly been limited to a few selected brain regions and frequency bands.

Here we propose a novel data-driven framework to estimate time-varying patterns of whole-brain functional network connectivity of resting state fMRI combined with the different frequencies and phase lags at which these patterns are observed. We show that this analysis identifies both broad-band cluster centroids that summarize connectivity patterns observed in many frequency bands, as well as clusters consisting only of functional network connectivity (FNCs) from a narrow range of frequencies along with associated phase profiles. The value of this approach is demonstrated by its ability to reveal significant group differences in males versus females regarding occupancy rates of cluster that would not be separable without considering the frequencies and phase lags. The method we introduce provides a novel and informative framework for analyzing time-varying and

Corresponding author. Phone: +1-505-414-0400. maziar@unm.edu, The Mind Research Network, 1101 Yale Blvd NE, Albuquerque, New Mexico 87106.

frequency specific connectivity which can be broadly applied to the study of the healthy and diseased human brain.

1 Introduction

Correlation analysis has been commonly used to study functional connectivity (FC) between brain regions. Such regions are either determined from regions-of-interest (ROIs) using prior anatomical knowledge (Biswal et al., 1995; Di Martino et al., 2008; Greicius et al., 2003) or through data-driven approaches, such as ICA, which looks for maximally spatially independent components (Beckmann et al., 2005; Calhoun et al., 2001; De Luca et al., 2006; Jafri et al., 2008; van de Ven et al., 2004). Regardless of the way such regions or components are derived, both FC and its close relative functional *network* connectivity (FNC)—referring to FC between component timecourses estimated by ICA—have been shown to be extremely informative about healthy and diseased brain function (Greicius, 2008; Koshino et al., 2005; Yu et al., 2011).

For example (Jafri et al., 2008) showed that functional network connectivity analysis of subjects during rest over the whole scan (i.e. temporally static functional network connectivity) reveals group differences between healthy controls and schizophrenia patients. More recently studies have moved beyond average FC/FNC to capture time-varying changes in connectivity (Calhoun et al., 2014). Sliding-window analysis has been a common strategy (Handwerker et al., 2012; Hutchison et al., 2013; Kiviniemi et al., 2011) which interestingly has been shown to be useful even in task-modulated data (Kucyi and Davis, 2014; Sako lu, 2010; Thompson et al., 2013) although other methods have also been suggested to capture dynamics such as instantaneous phase synchronization (Glerean et al., 2012) or spontaneous co-activation patterns analysis (CAP) (Liu and Duyn, 2013).

Moreover, spectral analysis of BOLD signal has shown promise for separating noise from neurophysiological sources of signals and in helping identify interesting differences within components of interest. As an example, (Allen et al., 2011) used the ratio of low-frequency power to high frequency power of ICA time courses to separate components contaminated by noise from meaningful resting state networks (RSNs). (Baria et al., 2011) showed that frequency contribution to BOLD signal power spectra varies based on spatial anatomical structures, consistent with other studies (He et al., 2010; Salvador et al., 2008; Zuo et al., 2010). Frequency differences between disease groups in components like the default mode network and others have also been identified (Calhoun et al., 2011; Garrity, 2007).

Other studies have analyzed spectral properties of correlation by estimating coherence. For example, (Cordes et al., 2001) suggested that by identifying frequencies contributing to observed correlation we can distinguish correlation due to respiratory and cardiac activity (which occurs around 0.1–0.5Hz and 0.6–1.2 Hz, respectively) from actual correlation

between auditory/visual/somatomotor regions which tends to have a lower frequency (< 0.1Hz) in coherence.

Coherence can be extended to study of temporal dynamics using time-frequency analysis such as short time Fourier transform (STFT), continuous wavelet transform or Empirical Mode Decomposition (EMD). These methods have been applied widely to EEG and MEG data (Duzel et al., 2003; Koenig et al., 2001; Miwakeichi et al., 2004) and to a smaller extent on fMRI datasets (Song et al., 2014). (Mehrkanoon et al., 2014) used time-frequency analysis of coherence of EEG rest data to find the 7 most stable connectivity networks in time-frequency domain using PCA. (Boonstra et al., 2007) used wavelet transform of surface electromyogram (EMG) signal to study dynamic change in power of EMG for their task-based study and (Schoffelen et al., 2005) used time-frequency coherence between motor cortex and spinal cord to study how it is affected by their designed reaction-time task. For fMRI data, in a relevant study, (Chang and Glover, 2010) used wavelet transform coherence (WTC) to show that coherence between default mode (DM) and task positive regions is considerably modulated in the time-frequency domain (frequency-wise the result is consistent with (Cordes et al., 2001)). All these studies suggest that brain region activations and correlations among them are in fact heterogeneous in their frequency spectra while also being temporally dynamic.

However there are limitations to each of these studies. For example although EEG/MEG data have the advantage of higher temporal resolution comparing to fMRI, their low spatial resolution limits the applicability of these analysis to study time-frequency coherence of whole brain regions. For example due to volume conduction artefact, (Mehrkanoon et al., 2014) had to remove the real part of the coherence, an issue that is not present with fMRI. On the other hand (Chang and Glover, 2010) focused on analysis of time-frequency coherence between a few selected brain regions in resting state fMRI using an ROI method and mainly studied differences in the dynamic nature of positive (in-phase) and negative (out-of-phase) coherence.

In this work we are interested in a whole brain analysis of the above properties. We chose ICA as a data-driven approach to identify functional networks of brain in the form of ICA components reflecting the within network connectivity with strong correlation. Compared to ROI methods with a fixed anatomical priors, we would expect to capture more functional variability across subjects while also taking advantage of ICA to further reduce noise susceptibility by removing components associated motion or physiological and imaging noise (Allen et al., 2011; Calhoun and Adali, 2012). Our work is built on top of the general framework of studying dynamics of brain connectivity during rest proposed by (Allen et al., 2014) which has also been used to study patient groups such as bipolar and schizophrenia patients (Damaraju et al., 2014b; Rashid et al., 2014). (Allen et al., 2014), similar to ours, is based on a spatial ICA decomposition of resting state data followed by sliding-window analysis but here we replace sliding-window analysis with a complex wavelet transform to be able to study FNCs in both the time and frequency domains.

The wavelet transform is a popular technique in time-frequency analysis. The kernel of the transform, referred to as a wavelet, is adapted to each frequency so that time-frequency

representation has higher temporal resolution in relatively higher frequencies. In the complex wavelet transform this kernel is complex and is used to estimate both amplitude and phase of signal at each time-frequency point.

Following to (Allen et al., 2014), k-means clustering was used as a way of summarizing observed FNCs and identifying recurring patterns of connectivity - here, however, in both the time and frequency domains. This has the direct advantage of simultaneously capturing temporal dynamics and frequency and phase profiles of each recurring FNCs (also referred to as connectivity states). We observed that some FNCs seem to have a similar connectivity patterns over a broader range of frequencies while others had a narrow frequency profile. Additionally, we observe that separation of states in the time-frequency plane enables us to find significant and interesting gender differences with respect to the occupancy rates of those identified states, states which would not be separable using domain-specific approaches, i.e. approaches that cluster patterns of time-varying connectivity in just the temporal or the spectral or the phase domain.

2 Materials and Methods

2.1 Materials and Preprocessing

We used same data as in (Allen et al., 2014). The data consists of resting-state fMRI scans of 405 healthy subjects (200 females and mean age of 21.0 years and ranging from 12 to 35 years). fMRI data was captured using the same scanner for all subjects, a 3-T Siemens Trio scanner with 12-channel radio frequency coil. T_2^*-weighted functional images were acquired using a gradient-echo EPI sequence with TE = 29 ms, TR = 2 s, flip angle = 75°, slice thickness = 3.5 mm and gap = 1.05 mm, FOV = 240 mm, matrix size = 64×64, voxel size = 3.75 mm × 3.75 mm × 4.55 mm and informed consent was obtained according to institutional guidelines at the University of New Mexico.

Pre-processing steps included discarding first 4 image volumes to avoid T1 equilibration effect, realignment, slice-timing correction, spatial normalization, reslicing to $3 \times 3 \times 3$ mm^3 voxels and spatial Gaussian smoothing (FWHM = 5 mm). And finally voxel time-series were z-scored to remove bias from further variance-dependent processes.

2.2 Group ICA and Postprocessing

GIFT implementation of Group-level Spatial ICA was used to estimate 100 functional networks as ICA components. First 120 subject-specific principal components were retained using PCA and concatenated and then 100 group PCs were estimated via second PCA. Infomax ICA was used to make these 100 PCs maximally spatially independent with 10 repetitions in ICASSO. Finally, aggregate spatial maps (SMs) were estimated as the modes of components clusters. GICA1 was used to back-reconstruct subject-specific SMs and time courses (TCs). 50 SMs related to physiological, motion and imaging artifacts were identified and removed from estimated set of SMs. The remaining subset of components is identified as intrinsic connectivity networks (ICNs) and has been used throughout the study. These are the components that have peak activations in grey matter and minimum spatial overlap with vascular, ventricular, motion and susceptibility artifacts. Also time courses are dominated by

low-frequency fluctuations. Figure S1 of appendix A represents aggregate SMs of identified ICNs.

Time courses of remaining SMs underwent post-processing to further reduce effects of noise which include detrending, motion regression and outlier removal. Please refer to (Allen et al., 2014) for more details on the above steps.

2.3 Frequency Analysis of Functional Network Connectivity over Time

We start our analysis by first looking at the frequency spectrum of FNC independent of time (temporally-static). This will help us better understand information we gain by analyzing both temporal dynamic and frequency variability of ICA time-courses connectivity through the proposed time-frequency approach.

A well-known approach to studying power spectral density of a signal is Welch's method (Welch, 1967), which is based on averaging of short Fourier transform of weighted segments of the input signal. Coherence between a pair of signals can be easily estimated as follows:

$$C_{xy}(f) = \frac{P_{xy}(f)}{\sqrt{P_{xx}(f)} \times \sqrt{P_{yy}(f)}} \quad \text{Equation 1}$$

Where $P_{xx}(f)$ and $P_{yy}(f)$ are power spectral densities of input signals x and y estimated using Welch's method and $P_{xy}(f)$ is the cross spectral densities of x and y estimated by element-wise Complex Conjugate Multiplication of signals' spectral densities.

Coherence between ICA time courses was calculated using the above equation over 5 equally spaced frequency bands in the interval [0.01,0.25]. To ensure valid comparisons of coherence across bands we z-scored coherence values based on the mean and standard deviation derived from a null distribution.

Separate null-distribution was created from each components pair and frequency band by estimated the coherence between time courses each belongs to a different subjects.

2.4 Time and Frequency analysis of Functional Network Connectivity

We need to modify Welch's method (Equation 1) to be able to capture temporal dynamics of coherence. First, inherent averaging over all periodograms (Fourier Transform of weighted segments of signal) is replaced by a local weighting function. Also, ideally, the size of these periodograms should be dependent on the local frequency content of the signal. To estimate low frequency content we need a relatively larger window size than the one to use to estimate higher frequency content. And at the end, when estimating time-frequency coherence between pairs of signals, smoothing function over time and frequency dimensions should be introduced to avoid bias toward unity coherence.

In our framework, we circumvent these issues by using an adaptive window size and by employing complex Morlet wavelets that have a Gaussian shape in the frequency domain.

The complex Morlet wavelet function is defined as $\frac{1}{\sqrt{2\pi}\sigma}e^{2\pi i f_c X} \times e^{-X^2/2\sigma^2}$, where X is the timeseries, f_c is the center frequency of the Morlet, and σ is the standard deviation of the Gaussian in the frequency domain. We set the standard deviation (σ) to be equal to 4.3 Hz and the Gaussian centers were equally spaced in the range of 0.01 and 0.25 Hz (0.01, 0.07, 0.13, 0.19, and 0.25 Hz)[1].

To accurately study frequency content of input time series at a given frequency of f, we must convolve the Morlet function centered at that frequency over time segments that have at least $0.5 \times \frac{1}{f \times T}$ timepoints, where T is the duration of the segment. For parts of convolution that do not span this length of input signal some padding is typically used which would result into contaminating the transformed result with invalid information. To avoid this problem we define a *cone of influence* which would only include estimations for which padding is not necessary.

In the following we explain steps of our proposed time-frequency analysis in more detail. Figure 1 provides a visual summary of all the steps.

2.4.1 Time-frequency coherence

One measure of time series dependency in the time-frequency domain is the Cross Wavelet Transform (XWT) (Torrence and Compo, 1998). It is the element-wise conjugate multiplication between coefficients of each time series in the transformed domain (Equation 2).

$$W^{xy} = W^x . \times W^y \quad \text{Equation 2}$$

Where W^x and W^y are wavelet transform of input signal x and y and $.\times$ represents element wise conjugate multiplication.

The above measure should be normalized by signal spectral power so that coherence estimation is not biased toward parts of the signal with more power. Additionally a smoothing function is introduced on this normalized measure to avoid bias toward unity. This smoothed and normalized measure is called a wavelet coherence transform (WTC) which is defined as follows:

$$R = \frac{S(W^{xy})}{\sqrt{S'(|W^x|^2)}\sqrt{S'(|W^y|^2)}} \quad \text{Equation 3}$$

Smoothing occurs in both time and frequency and is a function of frequency. This means that at different frequencies (or scales in the wavelet framework) we have different smoothing radii. Also in a more general form of WTC, the smoothing functions of the

---

[1]Note that our choice of wavelet kernels here is different from what is common in wavelet analysis. In typical wavelet analyses, all wavelets are driven from a mother wavelet but at a different scale and time as follows: $\psi_{s,\tau}(t) = \frac{1}{\sqrt{s}}\Psi\left(\frac{t-\tau}{s}\right)$ which defines a wavelet ψ at scale s and time τ from mother wavelet Ψ. Consequently the output would be a Scale x Time wavelet coefficients. However there is no uniform mapping from scaling to frequency. In fact, in our case, we use Morlet wavelet but instead of changing the scale we change its frequency center which has an explicit interpretation in frequency domain.

numerator and the denominator can be different (Mehrkanoon et al., 2011). We chose the general form of the WTC for our dependency measure and also selected uniform smoothing functions for both numerator and denominator, although weighted smoothing functions can be used as well.

We have also adapted the smoothing kernel size to the signal properties to maximize true time-frequency coherence estimation. In our implementation we looped through sets of possible smoothing parameters on simulated data modeled on the original input data and selected a set of parameters that best capture variation of coherence in time and frequency (More details are provided in Appendix E).

2.4.2 Cluster analysis—If we compute the wavelet coherence between all pairs of components of a specific subject at a specific time-frequency point, we have an estimation of FNC of that subject at that point. Based on the assumption that some connectivity patterns recur in time, here we extend the assumption to the frequency domain and search for FNC patterns that recur in both time and frequency domains. To achieve this, we concatenated estimated FNCs along subject-time-frequency (Figure 1) and used a k-means clustering algorithm to find a finite set of 'k' recurring FNCs.

For clustering analysis we set desired number of clusters equal to 5. Since our data is large and initial random assignment of the point to random selected clusters may bias the final clusters, we ran k-means 500 times on the same data with random initial guess of clusters assignment and we picked the clustering result which had the minimum sum of distances of each point to its corresponding cluster centroid.

Although the number of clusters is fixed here, in an additional analysis, we ran k-means clustering with different number of clusters in the range of 2–9 and we observed that cluster centroids at lower model orders is consistent with those obtained at higher model orders. Also estimation of the F-ratio with different number of clusters confirm our choice of k=5 (more details shown in Appendix B).

In a separate analysis, we ran k-means separately at each frequency band using same number of clusters. By using Sammon's non-linear mapping (Sammon, 1969) and projecting all the captured cluster centroids into a 2-d plane we observed that our original all-band k-means clusters spans the space of all band-specific clusters reasonably well. (More details in Appendix C).

3 Results

Our results include time-averaged multiband FNCs estimated by Welch's method (Figure 2) and connectivity states estimated as cluster centroids in time-frequency plane (Figure 3). Both types of FNCs are complex-valued, with time-lagged coherence conveyed by phase differences. Phase information is encoded with our selected circular colormap and amplitude is encoded as the lightness of the colors (lighter indicates smaller amplitude).

In Figure 2 we represent the average of band specific FNCs estimated using Welch's method over all subjects. For each frequency band, we show the average phase of coherence

(indicated by color hue) and average strength of coherence (indicated by color saturation) between each pair of components. We also display a polar histogram indicating distribution of the average phases for all pairs in the matrix.

By close inspection of band specific FNCs we conclude that some component-pair time courses have narrow band coherence. Specifically coherence between some Somatomotor and Visual components in second FNC of Figure 2 tend to appear in frequencies around 0.07Hz and attenuate in relatively lower and higher frequencies. The same situation is also true between cerebellar component time courses and many other component time courses. Also we can observe that the coherence phase of those component time courses is a function of frequency. For example, the cerebellar component time courses tend to be either positively or negatively correlated to some other components in the frequency range of (~0.01 *Hz*) and (~0.15 *Hz*) but are lagged ($having\ phase \sim +\frac{\pi}{2}$) and more uniform in the middle frequency range (~0.07 *Hz*).

It can also be observed that connectivity patterns of Figure 2 tend to have less visible structure in relatively higher range frequencies (~0.15 *Hz*). As mentioned in the methods section, because of the averaging in time in Welch's method, it is unclear if this lack of structure in that frequency range is due to low SNR or because of temporal dynamics nature of connectivity. The proposed time-frequency analysis allows us to investigate both frequency content and temporal behavior of the clusters.

In Figure 3 we represent cluster centroids as the estimated recurring functional connectivity states. States are sorted based on the associated rates of recurrence[2]. For each state we have a frequency histogram which shows at which range of frequencies a given state tends to recur. We also include a polar histogram indicating the distribution of coherence phases across all component pairs and frequencies. This plot represents the degree of time-lagged coherence between components in each state.

State 1 accounts for more than half of the observed FNCs which tend to appear in the frequency range of (~0.15 *Hz*) and have less phase variation. Relatively strong positive coherence (phase ~0) can be seen among somatomotor as well as visual networks. States 3 and 5 are the centroids of the clusters comprising narrow-band FNCs in the range of (~0.01 *Hz*) with visible variation in phase and with total occurrence of about 20%. Strong positive (in-phase) coherence among visual and part of cognitive control networks can be observed in state 3 and in state 5 this modulation expands to cover strong in-phase coherence between components in visual, somatomotor and auditory areas (the sensorimotor domain). In state 5, the sensorimotor domain has strong negative/out-of-phase (phase $\sim \pm \pi$) coherence with subcortical system which is clearly different from the same connectivity observed in state 3. States 2 and 4, on the other hand, have a wider distribution of frequencies, centered however on mid-range frequency of 0.07Hz and consequently having higher total occurrence rates than states 3 and 5.

---

[2]Since at each frequency band we a different length of cone of interest, we must correct for these lengths to accurately count number of recurrence of each state. To do so, we unwarp clustering results for each subject to have a square shape by replicating the initial and terminal elements, as shown in Appendix D.

Moreover, we can see that states 2 and 3 are visually similar to one another, but since we use both magnitude and phase of coherence in our k-means distance measure and the two states have different phase and amplitude histograms, they became the centroids of two distinct clusters. We have also been able to identify distinct cluster centroids with similar frequency ranges (State 2 and 4 both belong to frequency range of (~0.07 *Hz*) and State 3 and 5 both belong to a relatively lower range of frequencies (~0.01 *Hz*)). This is a direct result of having incorporated temporal dynamics as a separate dimension in our analysis.

State 4 which has a mid-range frequency histogram is extending our observation in the temporal-static and band specific FNC at 0.07Hz in Figure 2. In state 4 we also recognize mid-range frequency band (~0.07 *Hz*), phase lagged and synchronous coherence which was observed in second FNC in Figure 2 but also extending the coherence with same properties to other components pairs such as sub cortical-somatomotor and sub cortical-visual along with few other component pairs. In Figure 4 we represent observed coherence specific to state 4 between DM (Figure 4A, Right)/CB (Figure 4B, Right) to other selected networks and emphasize coherence differences regarding the phase and amplitude to same network pairs in State 2 (Figure 4A, Left)/CB (Figure 4B, Left) which spans relatively lower range of frequencies (~0.01Hz). This unique variation in coherence would have been identified only when we study coherence both in time and frequency domains.

3.1 Group differences

We also investigated gender differences regarding the occupancy of different states. For each subject and for each state we calculated occupancy rate of that state over the whole duration of the scan. The occupancy measure of a given state is just the percentage of time-frequency points that had been labeled with the cluster represented by the given state.

After regressing out age and motion parameters in the form of average translation and rotation from estimated occupancy rate, we perform a non-parametric Wilcoxon rank-sum test to compare occupancy rates between males and females. Uncorrected two-tailed p-values were 0.0004, 0.0129, 0.6672, 0.2895 and 0.3444 for states 1 to 5, respectively, providing strong evidence that males spent significantly more time in state 1 than females (mean ± SD: 49.5 ± 5.9 % vs 47.4 ± 7.2%). There is also some weak evidence that females spent more time in state 2 (23.2 ± 9.6% vs 21.1 ± 8.0% in males). To evaluate the robustness of these results, we also performed a split-half analysis on the data (balanced among randomly selected males and females) and observed that the overall finding and direction of the difference between groups stayed the same for both data sets which further supports the robustness of the comparison we conducted.

4 Discussion

In this work we investigated time-frequency sub-spaces spanned by the coherence among brain regions by first projecting the coherence into the time and frequency domain using WTC and then, by identifying clusters that coherence forms in the time-frequency domain using k-means clustering.

Chang et al., showed that the nature of coherence between default mode network (DMN) and the task positive network (TPN) is in fact temporally dynamic yet frequency specific. Consequently we expected to observe similar properties in statistical summaries (cluster centroids) of time-frequency varying measurements of whole brain connectivity. For example states 2 and 3 in Figure 3 have similar connectivity patterns and span frequency ranges of (~0.01 *Hz*) and (~0.15 *Hz*) respectively while states 4 and 5 have narrower range in their frequency profiles and unique connectivity patterns.

In another aspect of this work, we observed a significant difference between males and females in occupancy rates of the two most heavily occupied states. Interestingly, this was only possible because the states were separated along both time and frequency domain. Otherwise the overlap along either dimension would have obscured such an observation.

Moreover the complex nature of the chosen kernels enabled us to observe lagged coherence between input signals over the full range, from complete in-phase (0) coherence to complete out-of-phase ($\pm\pi$). Thus, clusters not only differ in the connectivity patterns they present and in underlying frequency content, but phase profiles also play an important roles in cluster formation. Common measures of correlation such as Pearson correlation and mutual information are unable to provide this level of resolution on phase-lagged coherence, although a sliding correlation windows lags (by shifting one time series relative to the other) have been suggested as a correlation-based approach to improving this resolution (Jafri et al., 2008).

Our results encompass a comprehensive set of functional components, obtained from the data using group spatial ICA. With our general framework it is still possible to identify regions among ICA components corresponding to ROIs selected by (Chang and Glover, 2010) but we have to keep in mind that Chang et al chose the wavelet scale as the representation of frequency in their time-frequency analysis of coherence. Scale is one of the parameters that is commonly used in wavelet analysis, which as with short-time or windowed Fourier analysis captures the rate of change of an input signal at a given time (or at a given *translation* of the wavelet kernel) window. However, the frequency bands of wavelets at each scale do not necessarily have same properties (e.g. usually they have different bandwidths) which makes it non-trivial to map scale to frequency. Another difference of our time-frequency analysis from the one used by (Chang and Glover, 2010) is that in our work the null-distribution has been derived from input data in contrast to the null-distribution estimated through Monte Carlo simulation employed by Chang et al. Finally we utilized a more general formulation of coherence as in Equation 3 and discovered through simulation that all of these choices resulted in a better performance that the one used by Chang with respect to sensitivity and specificity measures. More details on the simulation and performance comparison can be found in Appendix E.

This work can also be seen as an extension of (Allen et al., 2014) in which repetitive patterns of connectivity were identified along the time dimension. However (Allen et al., 2014) are unable to capture either the frequency profiles or lagged correlations associated to their recurring FNCs, while here we capture both properties.

Our work builds on existing treatments of functional network connectivity in several ways. First coherence analysis is based on an assumption that underlying sources of connectivity have frequency specificity, an assumption which is supported in resting state fMRI both by previous studies as well as our own analysis (see Figure 2). In non-dynamic coherence based studies, the observed connectivity patterns are averaged over time and dynamic connectivity states, i.e., states that recur reliably on shorter timescales, can be blurred out by averaging. In the case of resting state fMRI, this could lead to inaccurate estimation of functionally and behaviorally relevant connectivity patterns. Likewise, methods that do study dynamic correlation such as sliding-window analyses, look at connectivity states over all frequencies at once and are unable to locate connectivity states occurring primarily in specific sets of frequency bands. As with coherence analysis, sliding window dynamic correlation analyses can also lead to inaccurate or at least insufficiently refined estimation of connectivity in resting state fMRI.

Our analysis tackles both of these problems via a time-frequency coherence analysis employing frequency-adaptive window. The frequency specific and temporally dynamic nature of connectivity in resting state fMRI justifies application of our method in this study. Regarding the applicability of our method in other neuroscience studies, evaluation of the dynamic properties of the understudied connectivity both in time and frequency domains is needed. This includes study of frequency profiles of the observed connectivity to detect evidence of frequency specific sources of connectivity as well as investigating evidence for temporal dynamics of observed correlations versus an assumption of stationarity. A thorough preliminary analysis of spectral and dynamic features of the underlying data can both motivate a time-frequency analysis and also allow for interpretation of time-frequency results in relation to other available information. This can be useful, for example, in a task-based studies when we have frequency information on the task design (e.g. the frequency of the task stimuli). In such studies, using the additional information our method provides about the connectivity states, we can separate connectivity states that are not due to the task (states that have low-range frequency profiles relative to the frequency of the task design) and connectivity states that operate in frequencies that overlap with those of the task. And finally, good estimates of the SNR of the input signal are important for determining the parameters of Equation 3.

Additional studies are also needed to more thoroughly understand existing and possible formulations of coherence with respect, for example, to the kernel and smoothing functions, and to improve the reliability of estimated coherence.

4.1 Limitations and Future work

Limitations of this work include interpretability of the results and the methodological choice.

Regarding the interpretability, the nature of resting state data make it difficult to determine the true source of whole-brain connectivity patterns arising from different frequency profiles or distributions; it may have roots in physiological properties of spatial maps and differences in their activation, or could even be due to systematic noise during the scan.

In terms of interpretability, this work can be easily applied to task-based imaging studies, including those designed to capture cognitive states or to studies involving prior information on subject cognitive states (such as (Kucyi and Davis, 2014; Shirer et al., 2012)). It can also be extended to multimodal frameworks and applied in studies such as (Damaraju et al., 2015; Tagliazucchi et al., 2012; Yu et al., 2015), which could result in better neurophysiological interpretations of observed connectivity patterns. Also such work can help identify the relevance of the functional networks contributing to the observed FNCs under various conditions in order to better understand and interpret identified networks coherence behavior.

Effects of systematic noise on functional connectivity (either between regions or between networks), especially from motion, has been extensively studied (Power et al., 2012; Satterthwaite et al., 2012; Van Dijk et al., 2012). It has even been shown that motion effect on estimation of functional connectivity is not necessarily uniform; in large scale networks, it may induces significantly lower estimates than the actual correlation while it has the reverse effect on the actual correlation between smaller, more localized networks. ICA-based approaches appear to be more robust to these effects, though they are not immune (Damaraju et al., 2014a) and the proposed method might further mitigate some of these effects, by incorporating frequency and phase profiles to the connectivity measurements. Nonetheless, the impact of motion and scanner artifacts on time-frequency FNCs should be further investigated.

As always we are limited by our assumptions, and also methodological choices based on those assumptions.

Previous work, as well as our initial analysis of coherence, supports both the frequency specificity of functional connectivity in resting state fMRI combined and its temporally dynamic properties. This motivated us to develop a time-frequency coherence method designed to capture dynamically changing properties in both the time and frequency domains. However if the underlying assumptions regarding either frequency-specificity or temporal dynamics do not hold, this method may suffer from having less statistical power for estimating true time-frequency coherence. It is also worth mentioning that, theoretically, both a static coherence analysis and sliding-window correlation analysis can be computed from integral projection of the estimated time-frequency coherence along each dimension. Consequently we can obtain results of both methods by simply integrating estimated time-frequency coherence along time or frequency domain. In Figure 5, left, we show results using the pipeline proposed by (Allen et al., 2014) along with the one by integrating our estimated time-frequency coherence along frequency and then using cluster to find temporal dynamic connectivity states. On the right we compare connectivity states obtained by Welch's method (Figure 2) with results of integration of our estimated coherence along time over all subjects.

Another assumption is made in our choice of clustering algorithm. Here we have assumed that FNCs form clusters in the time-frequency domain that can be captured by k-means clustering, a method that looks for clusters with convex boundaries, although more complicated clustering approaches such as spectral clustering have been proposed to capture

more general shapes of clusters. Recent studies have also taken advantage of linear decomposition to break down observed FNCs into a finite number of connectivity patterns. For example (Leonardi et al., 2013) used PCA to linearly decomposed observed FNCs into finite set of connectivity patterns which are mutually spatially orthogonal and (Yaesoubi et al., 2015) looked for finite set of connectivity patterns that are mutually temporally independent and have linear contribution to the observed FNCs. CAP analysis as one of the more recent techniques to study dynamic connectivity has drawn the community's attention. CAP however, like many other approaches for dynamic connectivity analysis, is unable to capture frequency heterogeneity within the temporal dynamics. Future studies should investigate ways of integrating these decompositions in a broader approach to time-frequency analysis.

Lastly, there are many other approaches to studying time-frequency properties. Empirical mode decomposition (Huang et al., 1998), for example, estimates the instantaneous frequency of a given signal. Based on (Bruns, 2004), with correct settings, many time-frequency analyses can be made equivalent, so future studies might investigate the consistency of results across different approaches. Our framework does not limit us in the choice of the specific time-frequency analysis method, so any advances in this area would only strengthen the approach we propose as currently implemented.

5 Conclusion

In this work we have proposed a novel framework to study time-frequency dynamics of functional connectivity of resting-state fMRI data through a data-driven approach. Spatially independent components have been identified using spatial ICA, then the dynamic aspect of corresponding subject-specific functional network connectivity is studied in both time and frequency domains using wavelet transform coherence. Dynamic coherence of time courses is summarized by a finite number of recurring patterns of connectivity estimated by k-means clustering of the complex-valued FNCs. In this framework each FNC is in fact a snap shot of coherence between all pairs of ICA components at a time-frequency point. Through such analysis we can distinguish connectivity patterns recurring in a broader range of frequencies (although having different phase and amplitude profiles) from connectivity patterns that tend to be more narrow-band while retaining temporal dynamic property. Moreover, we observed that recurring connectivity patterns in time-frequency domain reveal significant group differences based on gender.

Supplementary Material

Refer to Web version on PubMed Central for supplementary material.

Acknowledgments

Abbreviations

ICA   Independent Component Analysis

FC   Functional Connectivity

FNC   Functional Network Connectivity

References

Allen EA, Damaraju E, Plis SM, Erhardt EB, Eichele T, Calhoun VD. Tracking Whole-Brain Connectivity Dynamics in the Resting State. Cereb Cortex. 2014; 24:663–676. [PubMed: 23146964]

Allen EA, Erhardt EB, Damaraju E, Gruner W, Segall JM, Silva RF, Havlicek M, Rachakonda S, Fries J, Kalyanam R, Michael AM, Caprihan A, Turner JA, Eichele T, Adelsheim S, Bryan AD, Bustillo J, Clark VP, Feldstein Ewing SW, Filbey F, Ford CC, Hutchison K, Jung RE, Kiehl KA, Kodituwakku P, Komesu YM, Mayer AR, Pearlson GD, Phillips JP, Sadek JR, Stevens M, Teuscher U, Thoma RJ, Calhoun VD. A baseline for the multivariate comparison of resting-state networks. Front Syst Neurosci. 2011; 5:2. [PubMed: 21442040]

Baria AT, Baliki MN, Parrish T, Apkarian AV. Anatomical and Functional Assemblies of Brain BOLD Oscillations. Journal of Neuroscience. 2011; 31:7910–7919. [PubMed: 21613505]

Beckmann CF, DeLuca M, Devlin JT, Smith SM. Investigations into resting-state connectivity using independent component analysis. Philosophical Transactions of the Royal Society B-Biological Sciences. 2005; 360:1001–1013.

Biswal B, Yetkin FZ, Haughton VM, Hyde JS. Functional connectivity in the motor cortex of resting human brain using echo-planar MRI. Magnetic Resonance in Medicine. 1995; 34:537–541. [PubMed: 8524021]

Boonstra TW, Daffertshofer A, Breakspear M, Beek PJ. Multivariate time-frequency analysis of electromagnetic brain activity during bimanual. motor learning. Neuroimage. 2007; 36:370–377. [PubMed: 17462913]

Bruns A. Fourier-, Hilbert- and wavelet-based signal analysis: are they really different approaches? J Neurosci Methods. 2004; 137:321–332. [PubMed: 15262077]

Calhoun VD, Adali T. Multisubject independent component analysis of fMRI: a decade of intrinsic networks, default mode, and neurodiagnostic discovery. IEEE Rev Biomed Eng. 2012; 5:60–73. [PubMed: 23231989]

Calhoun VD, Adali T, Pearlson GD, Pekar JJ. A method for making group inferences from functional MRI data using independent component analysis. Hum Brain Mapp. 2001; 14:140–151. [PubMed: 11559959]

Calhoun, Vince D.; Miller, R.; Pearlson, G.; Adal, T. The Chronnectome: Time-Varying Connectivity Networks as the Next Frontier in fMRI Data Discovery. Neuron. 2014; 84:262–274. [PubMed: 25374354]

Calhoun VD, Sui J, Kiehl K, Turner J, Allen E, Pearlson G. Exploring the psychosis functional connectome: aberrant intrinsic networks in schizophrenia and bipolar disorder. Front Psychiatry. 2011; 2:75. [PubMed: 22291663]

Chang C, Glover GH. Time-frequency dynamics of resting-state brain connectivity measured with fMRI. Neuroimage. 2010; 50:81–98. [PubMed: 20006716]

Cordes D, Haughton VM, Arfanakis K, Carew JD, Turski PA, Moritz CH, Quigley MA, Meyerand ME. Frequencies contributing to functional connectivity in the cerebral cortex in "resting-state" data. American Journal of Neuroradiology. 2001; 22:1326–1333. [PubMed: 11498421]

Damaraju, E.; AAE; Calhoun, V. Impact of head motion on ICA-derived functional connectivity measures. Biennial Conference on Resting State/Brain Connectivity; 2014a.

Damaraju E, Allen EA, Belger A, Ford J, McEwen SC, Mathalon D, Mueller B, Pearlson GD, Potkin SG, Preda A, Turner J, Vaidya JG, Van Erp T, Calhoun VD. Dynamic functional connectivity analysis reveals transient states of dysconnectivity in schizophrenia. Neuroimage: Clinical. 2014b

Damaraju, E.; Tagliazucchi, E.; Laufs, H.; Calhoun, V. Dynamic functional network connectivity from rest to sleep. OHBM; Honolulu, HI: 2015.

De Luca M, Beckmann CF, De Stefano N, Matthews PM, Smith SM. fMRI resting state networks define distinct modes of long-distance interactions in the human brain. Neuroimage. 2006; 29:1359–1367. [PubMed: 16260155]

Di Martino A, Scheres A, Margulies DS, Kelly AM, Uddin LQ, Shehzad Z, Biswal B, Walters JR, Castellanos FX, Milham MP. Functional connectivity of human striatum: a resting state FMRI study. Cereb Cortex. 2008; 18:2735–2747. [PubMed: 18400794]

Duzel E, Habib R, Schott B, Schoenfeld A, Lobaugh N, McIntosh AR, Scholz M, Heinze HJ. A multivariate, spatiotemporal analysis of electromagnetic time-frequency data of recognition memory. Neuroimage. 2003; 18:185–197. [PubMed: 12595175]

Garrity. Aberrant 'default mode' functional connectivity in schizophrenia (vol 164, pg 450, 2007). American Journal of Psychiatry. 2007; 164:1123–1123.

Glerean E, Salmi J, Lahnakoski JM, Jääskeläinen IP, Sams M. Functional Magnetic Resonance Imaging Phase Synchronization as a Measure of Dynamic Functional Connectivity. Brain Connect. 2012; 2:91–101. [PubMed: 22559794]

Greicius M. Resting-state functional connectivity in neuropsychiatric disorders. Curr Opin Neurol. 2008; 21:424–430. [PubMed: 18607202]

Greicius MD, Krasnow B, Reiss AL, Menon V. Functional connectivity in the resting brain: a network analysis of the default mode hypothesis. Proc Natl Acad Sci U S A. 2003; 100:253–258. [PubMed: 12506194]

Grinsted A, Moore JC, Jevrejeva S. Application of the cross wavelet transform and wavelet coherence to geophysical time series. Nonlinear Processes in Geophysics. 2004; 11:561–566.

Handwerker DA, Roopchansingh V, Gonzalez-Castillo J, Bandettini PA. Periodic changes in fMRI connectivity. Neuroimage. 2012; 63:1712–1719. [PubMed: 22796990]

He BYJ, Zempel JM, Snyder AZ, Raichle ME. The Temporal Structures and Functional Significance of Scale-free Brain Activity. Neuron. 2010; 66:353–369. [PubMed: 20471349]

Huang NE, Shen Z, Long SR, Wu MLC, Shih HH, Zheng QN, Yen NC, Tung CC, Liu HH. The empirical mode decomposition and the Hilbert spectrum for nonlinear and non-stationary time series analysis. Proceedings of the Royal Society a-Mathematical Physical and Engineering Sciences. 1998; 454:903–995.

Hutchison RM, Womelsdorf T, Gati JS, Everling S, Menon RS. Resting-state networks show dynamic functional connectivity in awake humans and anesthetized macaques. Hum Brain Mapp. 2013; 34:2154–2177. [PubMed: 22438275]

Jafri MJ, Pearlson GD, Stevens M, Calhoun VD. A method for functional network connectivity among spatially independent resting-state components in schizophrenia. Neuroimage. 2008; 39:1666–1681. [PubMed: 18082428]

Kiviniemi V, Vire T, Remes J, Elseoud AA, Starck T, Tervonen O, Nikkinen J. A sliding time-window ICA reveals spatial variability of the default mode network in time. Brain Connect. 2011; 1:339–347. [PubMed: 22432423]

Koenig T, Marti-Lopez F, Valdes-Sosa P. Topographic time-frequency decomposition of the EEG. Neuroimage. 2001; 14:383–390. [PubMed: 11467912]

Koshino H, Carpenter PA, Minshew NJ, Cherkassky VL, Keller TA, Just MA. Functional connectivity in an fMRI working memory task in high-functioning autism. Neuroimage. 2005; 24:810–821. [PubMed: 15652316]

Kucyi A, Davis KD. Dynamic functional connectivity of the default mode network tracks daydreaming. Neuroimage. 2014; 100:471–480. [PubMed: 24973603]

Leonardi N, Richiardi J, Gschwind M, Simioni S, Annoni JM, Schluep M, Vuilleumier P, Van De Ville D. Principal components of functional connectivity: a new approach to study dynamic brain connectivity during rest. Neuroimage. 2013; 83:937–950. [PubMed: 23872496]

Liu X, Duyn JH. Time-varying functional network information extracted from brief instances of spontaneous brain activity. Proceedings of the National Academy of Sciences of the United States of America. 2013; 110:4392–4397. [PubMed: 23440216]

Mehrkanoon S, Breakspear M, Boonstra TW. Low-Dimensional Dynamics of Resting-State Cortical Activity. Brain Topography. 2014; 27:338–352. [PubMed: 24104726]

Mehrkanoon S, Breakspear M, Daffertshofer A, Boonstra T. Generalized time-frequency coherency for assessing neural interactions in electrophysiological recordings. Nature Precedings. 2011

Miwakeichi F, Martinez-Montes E, Valdes-Sosa PA, Nishiyama N, Mizuhara H, Yamaguchia Y. Decomposing EEG data into space-time-frequency components using Parallel Factor Analysis. Neuroimage. 2004; 22:1035–1045. [PubMed: 15219576]

Power JD, Barnes KA, Snyder AZ, Schlaggar BL, Petersen SE. Spurious but systematic correlations in functional connectivity MRI networks arise from subject motion. Neuroimage. 2012; 59:2142–2154. [PubMed: 22019881]

Rashid B, Damaraju E, Pearlson GD, Calhoun VD. Dynamic Connectivity States Estimated from Resting fMRI Identify Differences among Schizophrenia, Bipolar Disorder, and Healthy Control Subjects. Frontiers in Human Neuroscience. 2014; 8

Sako lu Ü, Pearlson Godfrey D, Kiehl Kent A, Michelle Wang Y, Michael Andrew M, Calhoun Vince D. A method for evaluating dynamic functional network connectivity and task-modulation: application to schizophrenia. Magnetic Resonance Materials in Physics, Biology and Medicine. 2010; 23:351–366.

Salvador R, Martinez A, Pomarol-Clotet E, Gomar J, Vila F, Sarro S, Capdevila A, Bullmore ET. A simple view of the brain through a frequency-specific functional connectivity measure. Neuroimage. 2008; 39:279–289. [PubMed: 17919927]

Sammon JW. A Nonlinear Mapping for Data Structure Analysis. Ieee Transactions on Computers C. 1969; 18:401.

Satterthwaite TD, Wolf DH, Loughead J, Ruparel K, Elliott MA, Hakonarson H, Gur RC, Gur RE. Impact of in-scanner head motion on multiple measures of functional connectivity: Relevance for studies of neurodevelopment in youth. Neuroimage. 2012; 60:623–632. [PubMed: 22233733]

Schoffelen JM, Oostenveld R, Fries P. Neuronal coherence as a mechanism of effective corticospinal interaction. Science. 2005; 308:111–113. [PubMed: 15802603]

Shirer WR, Ryali S, Rykhlevskaia E, Menon V, Greicius MD. Decoding subject-driven cognitive states with whole-brain connectivity patterns. Cereb Cortex. 2012; 22:158–165. [PubMed: 21616982]

Song XP, Zhang Y, Liu YJ. Frequency Specificity of Regional Homogeneity in the Resting-State Human Brain. Plos One. 2014; 9

Tagliazucchi E, von Wegner F, Morzelewski A, Brodbeck V, Laufs H. Dynamic BOLD functional connectivity in humans and its electrophysiological correlates. Front Hum Neurosci. 2012; 6:339. [PubMed: 23293596]

Thompson GJ, Magnuson ME, Merritt MD, Schwarb H, Pan WJ, McKinley A, Tripp LD, Schumacher EH, Keilholz SD. Short-Time Windows of Correlation Between Large-Scale Functional Brain Networks Predict Vigilance Intraindividually and Interindividually. Hum Brain Mapp. 2013; 34:3280–3298. [PubMed: 22736565]

Torrence C, Compo GP. A practical guide to wavelet analysis. Bulletin of the American Meteorological Society. 1998; 79:61–78.

van de Ven VG, Formisano E, Prvulovic D, Roeder CH, Linden DEJ. Functional connectivity as revealed by spatial independent component analysis of fMRI measurements during rest. Hum Brain Mapp. 2004; 22:165–178. [PubMed: 15195284]

Van Dijk KRA, Sabuncu MR, Buckner RL. The influence of head motion on intrinsic functional connectivity MRI. Neuroimage. 2012; 59:431–438. [PubMed: 21810475]

Welch PD. The use of fast Fourier transform for the estimation of power spectra: A method based on time averaging over short, modified periodograms. Audio and Electroacoustics, IEEE Transactions on. 1967; 15:70–73.

Yaesoubi M, Miller RL, Calhoun VD. Mutually temporally independent connectivity patterns: A new framework to study the dynamics of brain connectivity at rest with application to explain group difference based on gender. Neuroimage. 2015; 107:85–94. [PubMed: 25485713]

Yu Q, Sui J, Rachakonda S, He H, Gruner W, Pearlson G, Kiehl KA, Calhoun VD. Altered topological properties of functional network connectivity in schizophrenia during resting state: a small-world brain network study. Plos One. 2011; 6:e25423. [PubMed: 21980454]

Yu, Q.; Wu, L.; Bridwell, D.; Erhardt, EB.; Du, Y.; He, H.; Sui, J.; Pearlson, G.; Calhoun, V. Concurrent EEG-fMRI multi-modal brain graph. OHBM; Honolulu HI: 2015.

Zuo XN, Di Martino A, Kelly C, Shehzad ZE, Gee DG, Klein DF, Castellanos FX, Biswal BB, Milham MP. The oscillating brain: Complex and reliable. Neuroimage. 2010; 49:1432–1445. [PubMed: 19782143]

8 Appendices

8.1 Appendix A

In following we are showing spatial maps of all 50 ICA components identified as intrinsic connectivity networks and used in this study. Sagittal, coronal and axial slices for each SM is shown. More detailed information on these ICNs can be find in supplementary material of (Allen et al., 2014).

8.2 Appendix B

We ran k-means clustering with different number of clusters and observed that by running clustering with enough number of iterations for each choice of 'k', the result cluster centroids are reasonably consistent from low to high model order.

Figure S2 shows k-means centroids for *k* ranging from 2 to 9.

Our choice of 'k' in this study was based on the inspection of f-ratio for each 'k' in the above range. F-ration here is defined as the average ratio of sum of squared distance between each cluster points and the corresponding cluster centroids (inside cluster dispersion) to the sum of square distance of the points outside of the cluster to the same estimated centroids (outside cluster dispersion).

We want to minimize this measure with minimum possible number of clusters so we look for 'k's on the elbow of the f-ratio curve which here is k=5 (Figure S2B).

8.3 Appendix C

Since we are running k-means on a large number of data point and looking for few centroids, there is a high probability to reach a local minimum solution based on the initial guess and that is the main reason we ran k-means 500 times each with a different initial guess of the solution. In addition to this we also decided to run k-means separately on parts of the data that correspond to different frequency bands. Since we have 5 frequency bands, we would have 25 k-means centroids (5 for each band). By using Sammon non-linear mapping (Sammon, 1969) we mapped all 25 centroids into a 2-d plane to get a sense of the space they have spanned. Figure … has summarized this analysis. The bottom side of this hexagon represents centroids of the main k-means clustering. Other sides, each corresponds to single band k-means centroids sorted by their recurrence rate (1 is the highest recurring centroid and 5 is the lowest one). Inside of the hexagon is the result of Sammon mapping of

centroids into a 2-d plane. We can clearly see that main k-means centroids (blue circle) fairly cover the space spanned by other centroids.

8.4 Appendix D

To accurately account for the occurrence rate of states across frequency band the coin of interests for each band should be expanded (unwarped) to span the whole duration of the scan. The unwarping uses nearest neighbor interpolation on the cluster labels to fit the warped time-frequency plane to a square as follows:
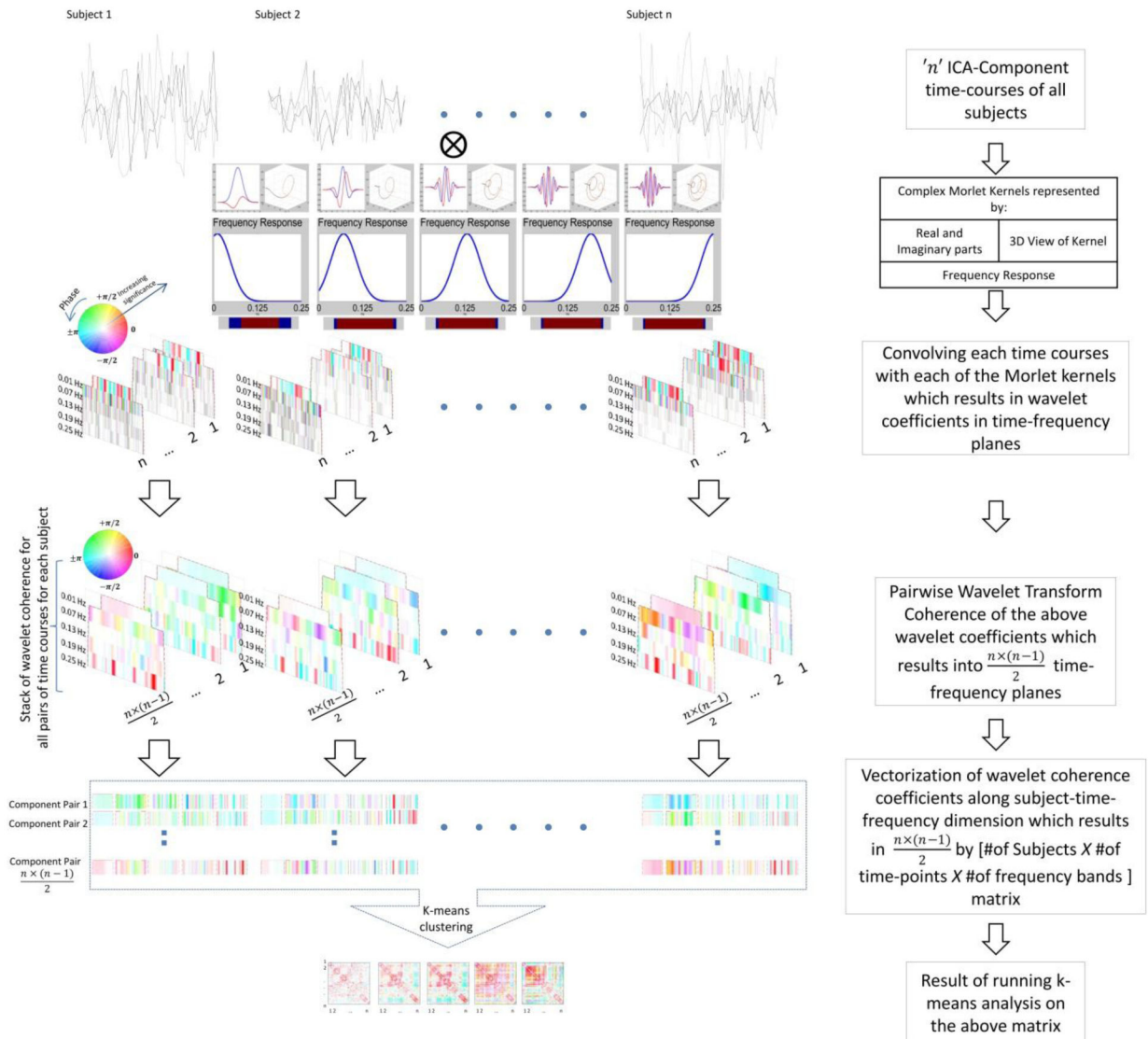
8.5 Appendix E

To study performance of our method in compare to wavelet coherence transform implementation of (Grinsted et al., 2004) as well as to find the optimal setting in general formulation of wavelet coherence in Equation 3 we simulated pair of time series with dynamic coherence both in time and frequency.

360s long simulated time series are sampled with TR=2s same as fMRI time courses. The pair of time series is correlated at frequency 0.07 Hz during the first third of the duration and at 0.19 Hz during the last third of the duration of the signals.

We used sensitivity and specificity as two quantitative measures to study performance of the general wavelet coherence formulation under different settings. As in (Mehrkanoon et al., 2011) sensitivity is defined as the ratio of correctly recognized significant coherence to the all truly significant coherence. Specificity is defined similarly but as the ratio of correctly recognize insignificant coherence to the all truly insignificant coherence. We desire to maximize both at the same time. The significance level was selected as the 90th percentile of null distribution. The null distribution was estimated by surrogating 500 pairs of time series with above properties. Also sensitivity and specificity have been averaged over 500 runs of wavelet coherence analysis. The parameters of Equation 3 than we looped through are radius of S and S' along time and frequency dimensions while size of S is always smaller than S' in both dimensions.

Highlights

- Design of a framework for time-frequency analysis of coherence in rest fMRI data

- We study time-frequency coherence in form of functional network connectivity (FNC)

- Enables us to jointly study temporal dynamics spectral power and phase profiles of FNCs

- Identification of clusters formed by such FNCs in the time-frequency domain

- Reveals significant gender differences based on occupancy measures of each cluster

Figure 1.
Pipeline of the proposed framework to find repetitive patterns of connectivity in time-frequency domain: First input time courses are transformed into time-frequency domain using Complex mortlet kernels. Then coherence in that domain is calculated using Wavelet Transform Coherence. As the last step, k-means clustering is used to find clusters of FNCs along time and frequency dimension.
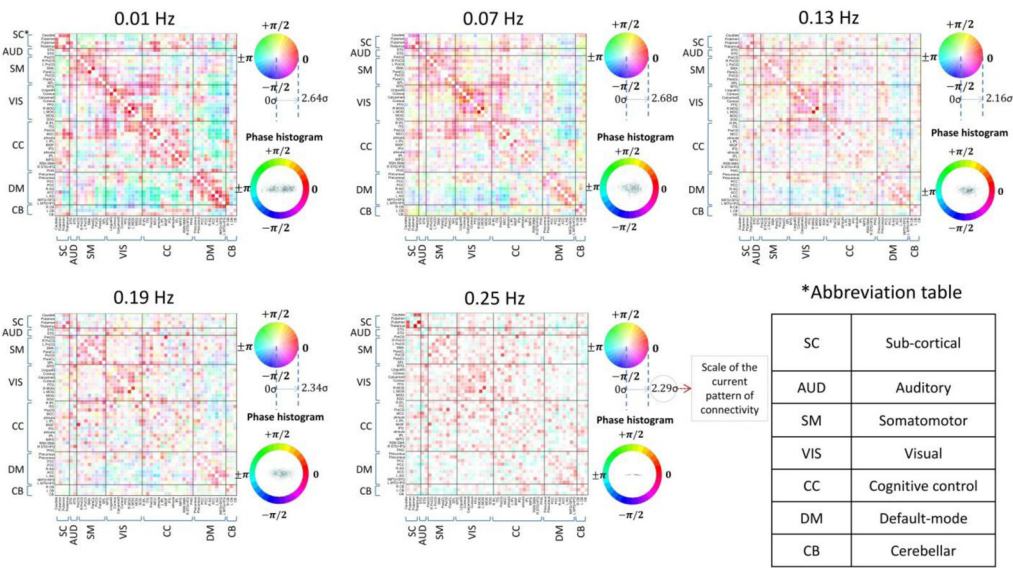
Figure 2.
Connectivity patterns between components associated with each selected frequency bands integrated over time. As clearly visible, less connectivity structure can be observed in relatively higher frequencies. However due to the integration over time the source of this lack of structure is not obvious in this analysis. Identified functional networks as well as their odering here are the same as reported in (Allen et al., 2014). Please refer to Figure S1 in appendix A for a full display of each component.
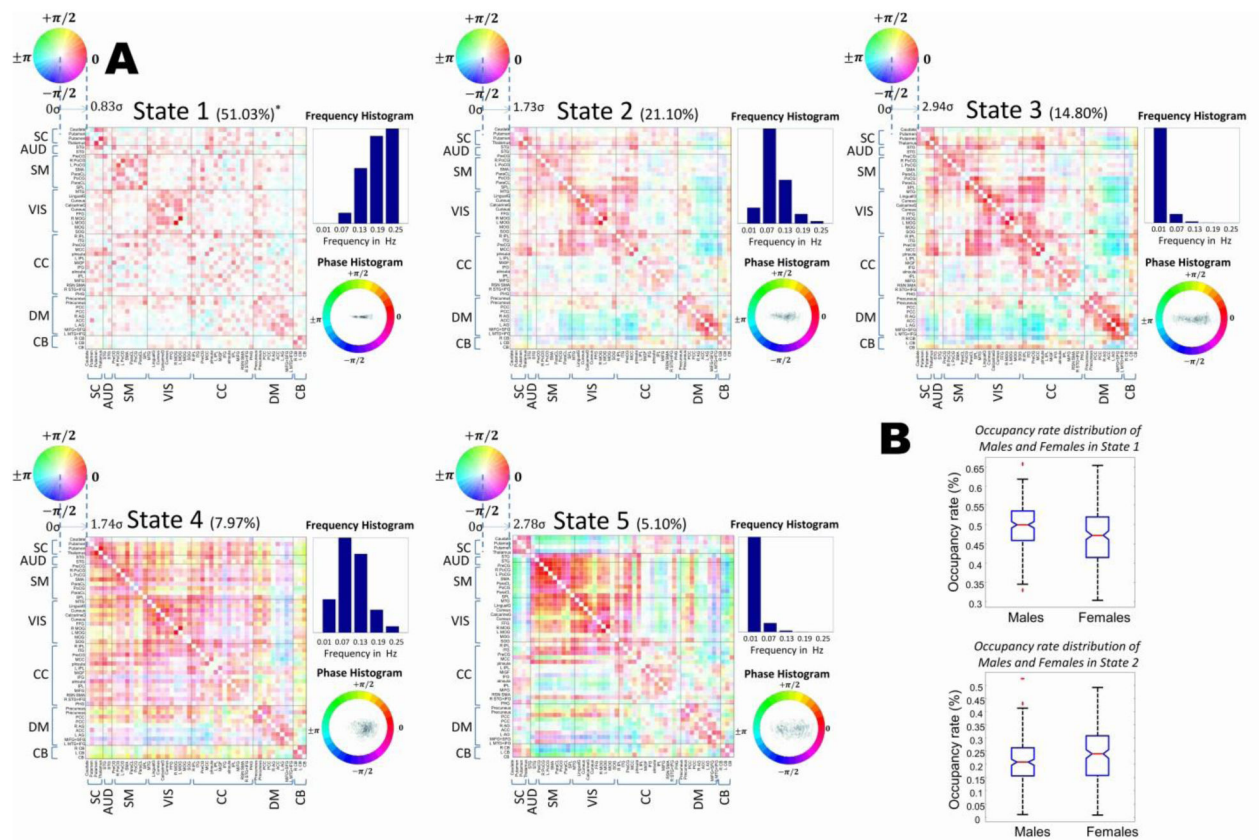
Figure 3.
(A) Repetitive patterns of connectivity estimated as the cluster centroids formed in time-frequency domain. These patterns (States) are sorted based on their occurrence rates and for each pattern, frequency and phase histogram is presented. (B) Box plots for occupacy rate distribution of males and females for two most reccuring states. These two states are the ones in which significant differences between occupancy rates of males and females have been observed.
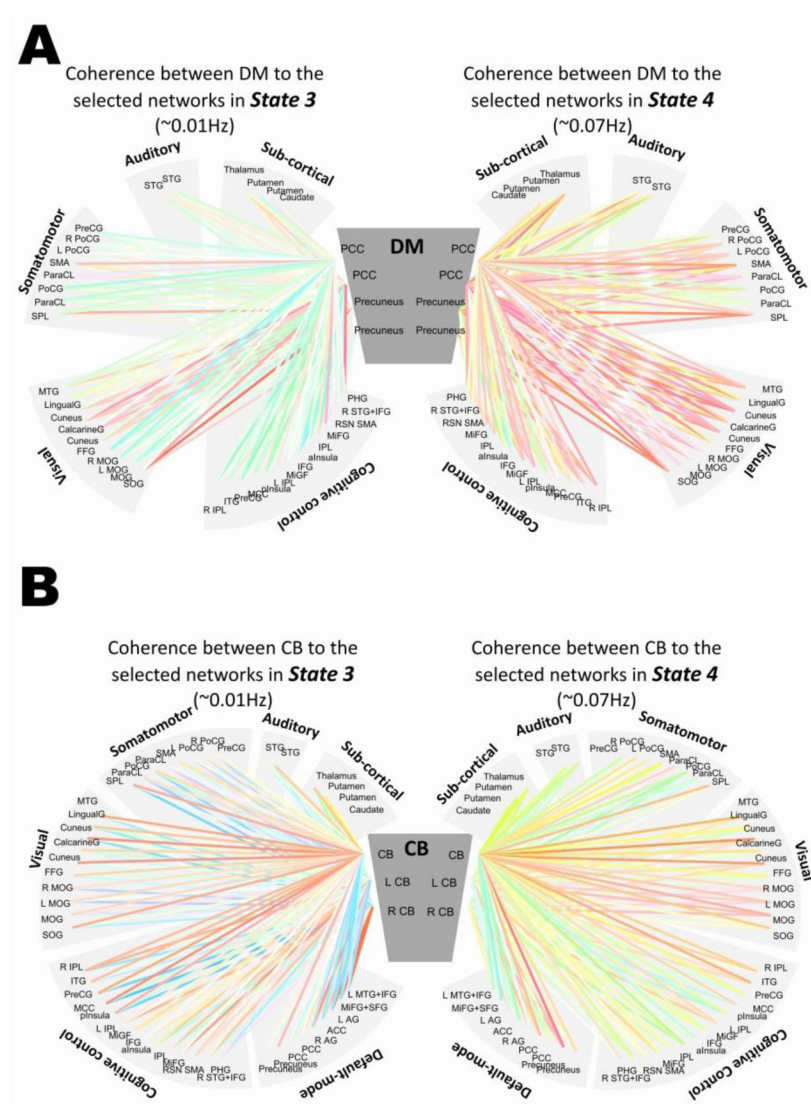
Figure 4.
In this figure we emphasize the difference in the nature of coherence based on its phase and amplitude observed in state 3 [Left] (with relatively lower range frequency profile (~0.01Hz)) comparing to state 4 [Right] (with frequency range ~ 0.07Hz) between (A) Default Mode networks and other selected networks and (B) Cerebellar networks and the rest of the networks.
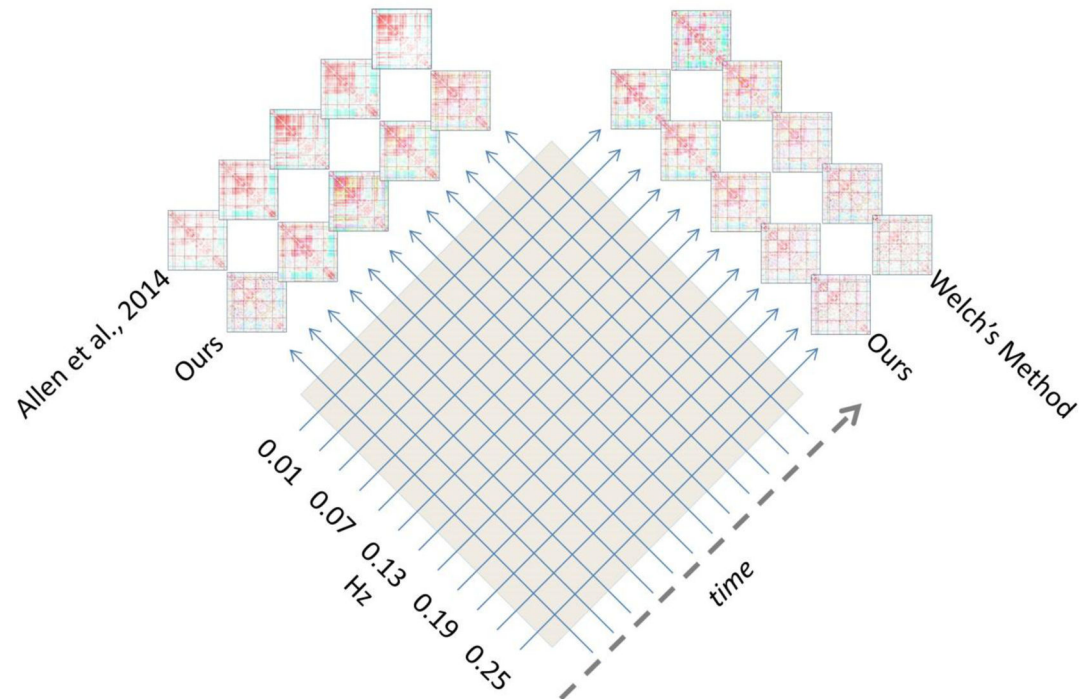
Figure 5.
Integral projection of our estimated time-frequency coherence along time and frequency would lead to similar results by sliding-window analysis (Allen et al., 2014) and coherence analysis, respectively. However as mentioned above, any of these methods may inaccurately estimatie the connectivity if their corresponding underlyding assumptions do not hold in real data.